Acta Crystallographica Section D
Biological Crystallography
ISSN 0907-4449

Structure of *Escherichia coli* pyridoxine 5′-phosphate oxidase in a tetragonal crystal form: insights into the mechanistic pathway of the enzyme

Martin K. Safo,[a]* Faik N. Musayev[a] and Verne Schirch[b]

[a]Department of Medicinal Chemistry, Virginia Commonwealth University, Richmond, Virginia 23219, USA, and [b]Department of Biochemistry and Institute for Structural Biology and Drug Discovery, Virginia Commonwealth University, Richmond, Virginia 23219, USA

Correspondence e-mail: msafo@mail2.vcu.edu

Received 21 December 2004
Accepted 18 February 2005

PDB Reference: pyridoxine 5′-phosphate oxidase, 1wv4, r1wv4sf.

Escherichia coli pyridoxine 5′-phosphate oxidase (ePNPOx) catalyzes the terminal step in the biosynthesis of pyridoxal 5′-phosphate (PLP) by the FMN oxidation of pyridoxine 5′-phosphate (PNP) or pyridoxamine 5′-phosphate (PMP), forming $FMNH_2$ and H_2O_2. The crystal structure of ePNPOx is reported in a tetragonal unit cell at 2.6 Å resolution. The three-dimensional fold of this structure is very similar to those of the *E. coli* and human enzymes that crystallized in trigonal and monoclinic unit cells. However, unlike the previous structures, the tetragonal structure shows major disorder in one of the two subunit domains that has opened up both the active site and a putative tunnel. Comparison of these structures gives an insight into the mechanistic pathway of PNPOx: from the resting enzyme with no substrate bound, to the initial binding of the substrate at the active site, to the catalytic stage and to the release of the catalytic product from the active site.

1. Introduction

Pyridoxine 5′-phosphate oxidase catalyzes the terminal step in the biosynthesis of PLP by oxidizing the 4′-hydroxyl group of PNP or the 4′-amino group of PMP to an aldehyde, forming PLP with the transfer of two electrons to oxygen from FMN (Zhao & Winkler, 2000; Hill *et al.*, 1996).

Key questions concern the mechanism of oxidation of PNP or PMP to PLP and how the reactive PLP is regulated and transferred from PNPOx to vitamin B_6 apoenzymes to form catalytically active B_6 holoenzymes. Recent studies indicate that the mechanism of oxidation involves a stereospecific hydride-ion transfer between C4′ of PLP and N5 of FMN (Di Salvo *et al.*, 2002). Other studies also suggest that in addition to the active site, PNPOx contains a non-catalytic site that binds PLP tightly, which dissociates very slowly since repeated chromatography on size-exclusion columns does not separate PNPOx from the non-catalytic bound PLP (Yang & Schirch, 2000; Musayev *et al.*, 2003). Interestingly, this slowly dissociating PLP could be readily transferred to apo serine hydroxymethyltransferase (SHMT) to form the active holoenzyme.

Pyridoxal 5′-phosphate contains a very reactive aldehyde group that reacts with virtually all nucleophiles in the cell. In its function in the cell as a cofactor for many enzymes involved in amino-acid metabolism, PLP is bound as an internal aldimine to an ε-amino group of a lysyl residue at the active site (John, 1998*a*,*b*). This is protected from most nucleophiles in

the cell, so that only the substrate amino group can form the active-site complex as an external aldimine. This suggests that during the biosynthesis of PLP in *Escherichia coli*, the reactive aldehyde group must be protected from forming non-productive complexes with other nucleophiles and proteins so that it can be targeted directly to those apoenzymes that require it for activity. Channeling, which avoids releasing such reactive or unstable molecules to be free in the cell cytoplasm, has been suggested for PLP transfer (Ováldi & Srere, 2000). However, there has been little physical evidence showing direct interaction between channeling enzymes and most of the evidence for channeling derives from controversial kinetic studies.

Several crystal structures of PNPOx have recently been determined and published, including an ePNPOx binary complex with FMN in a trigonal unit cell (Safo *et al.*, 2000) and ePNPOx ternary complexes with FMN and PLP in trigonal (Safo *et al.*, 2001) and monoclinic unit cells (Di Salvo *et al.*, 2002), as well as a human PNPOx ternary complex with FMN and PLP in a trigonal unit cell (Musayev *et al.*, 2003). The active-site conformations are different in these crystal structures, with the unliganded trigonal form showing an open conformation, while the liganded trigonal and monoclinic forms show partially and completely closed conformations, respectively.

We now report another ePNPOx structure in a tetragonal unit cell that shows major disorder. Comparison of all three crystal forms allows systematic observations of reaction cycles that may explain on a molecular level the mechanistic pathway of PNPOx: from the resting enzyme with no substrate bound, to the initial binding of PNP at the active site (pre-reaction state), to the catalytic stage and finally to the transfer of the catalytic product PLP from the active site for subsequent transfer to vitamin B_6 apoenzymes.

2. Materials and methods

2.1. Crystallization, data collection and structure determination

PNPOx was purified from *E. coli* as described previously (Di Salvo *et al.*, 1998). FMN binds tightly and co-purified with the protein, therefore no additional FMN was added during the crystallization experiments. The tetragonal crystals were obtained when equal volumes of protein solution (5 mg ml^{-1}) in 100 m*M* K_2PO_4 pH 7.5 with 5 m*M* 2-mercaptoethanol were mixed with reservoir solution containing 60 m*M* HEPES buffer pH 6.8 and 0.65 *M* $KH_2PO_4/NH_4H_2PO_4$. The tetragonally shaped crystals reached their maximum dimensions (0.40 × 0.20 × 0.10 mm) in about 4–5 weeks. A diffraction data set was collected at 100 K using a Molecular Structure Corporation (MSC) X-Stream Cryogenic Crystal Cooler System, an R-AXIS II image-plate detector equipped with Osmic confocal mirrors and a Rigaku RU-200 X-ray generator operating at 50 kV and 100 mA. Prior to use in X-ray diffraction, the crystals were first washed in a cryoprotectant solution containing 2.1 *M* $KH_2PO_4/NH_4H_2PO_4$, 0.1 *M* Na HEPES buffer H 8.0 and 4% glycerol and then transferred stepwise to similar solutions containing 8 and 12% glycerol. The data were processed using *BIOTEX* software (MSC) and the *CCP*4 suite (Collaborative Computational Project, Number 4, 1994). Statistics for the data set are listed in Table 1.

Table 1
Crystal information, data-collection and refinement parameters for ePNPOx in a tetragonal unit cell.

Values in parentheses refer to the outermost resolution bin.

Data-collection statistics	
Unit-cell parameters (Å)	$a = b = 54.42$, $c = 164.42$
Resolution (Å)	45.38–2.6 (2.8–2.6)
No. of measurements	59668 (11373)
No. of unique reflections	14262 (2819)
$I/\sigma(I)$	12.4 (2.7)
Completeness (%)	90.8 (91.3)
$R_{\rm merge}$† (%)	6.3 (24.9)
Structure refinement	
Resolution limit (Å)	45.38–2.6 (2.76–2.6)
No. of reflections	14120 (2285)
Completeness	96.2
R factor (%)	24.2 (29.2)
$R_{\rm free}$‡ (%)	29.0 (36.9)
R.m.s.d. from standard geometry	
Bond lengths (Å)	0.022
Bond angles (°)	2.1
Dihedral angles	
Most favored regions	83.3
Additional allowed regions	16.0
Average *B* values (Å^2)	
All non-H atoms	53.9
Protein atoms	53.8
FMN	56.5
Phosphate	97.4
Water	54.1

† $R_{\rm merge} = \sum\langle I\rangle - I/\sum I$. ‡ The 5% of the reflections that were used for the calculation of $R_{\rm free}$ were excluded from the refinement.

The tetragonal crystal structure was determined by molecular-replacement methods using the program *AMoRe* from the *CCP*4 suite (Collaborative Computational Project, Number 4, 1994). Based on the solvent content of the unit cell (~46%), we expected a dimer of ePNPOx in the asymmetric unit. The monomeric trigonal structure of ePNPOx (PDB code 1g79; residues 20–218), omitting all FMN, PLP, phosphate and water molecules, was used as the search model. The cross-rotation function was calculated using normalized structure factors with data in the resolution range 8.0–4.0 Å. Two unique peaks with correlation coefficients of 0.23 and 0.19 were observed. A translation function followed by rigid-body refinement for space group $P4_1$ resulted in correlation coefficients of 0.34 and 0.32 and *R* factors of 47.9 and 48.2%, respectively. The solutions correspond to the two dimer halves (monomers *A* and *B*) of the molecule.

Structure refinement was performed with *CNS* (Brünger *et al.*, 1998), with overall anisotropic *B*-factor correction and bulk-solvent correction. A statistically random selection of 5% of the total reflection data was excluded from the refinement and used to calculate the free *R* factor ($R_{\rm free}$) as a monitor of model bias (Brünger, 1992). The starting model was subjected to rigid-body and positional refinement with the 2.6 Å crystallographic data to an *R* factor and $R_{\rm free}$ of 40.3 and 48.6%,

respectively. The model resulted in clear density for the FMN, which was modeled into the map. On the other hand, residues 134–175 and 135–172 of monomers *A* and *B*, respectively, showed very weak or no density and were deleted from the model. The model was then submitted to a round of rigid-body, positional and simulated-annealing refinement to an *R* factor and $R_{\rm free}$ of 36.3 and 43.6%, respectively. The resulting electron-density maps showed densities for the N-terminal amino-acid residues 11–19 and 17–19 for monomers *A* and *B*, respectively, and were included in the model. The positions of several of the residues were also corrected manually. Several alternate rounds of positional, simulated-annealing and individual *B*-factor refinement with the addition of two phosphate and 72 water molecules resulted in a model with *R*-factor and $R_{\rm free}$ values of 24.2 and 29.0% for data above $1.0\sigma(F)$. All model building and corrections were carried out using the program *TOM* (Cambillau & Horjales, 1987). Refinement statistics are summarized in Table 1.

3. Results and discussion

3.1. Crystal structure of ePNPOx in a tetragonal unit cell

The final model has two monomers in the asymmetric unit containing 316 amino-acid residues of the possible 436 amino acids, two FMN cofactors, two phosphates and 72 water molecules. The two monomers in the asymmetric unit of the tetragonal structure constitute a functional dimer and interact extensively along one-half of each monomer as previously discussed (Safo *et al.*, 2000, 2001; Di Salvo *et al.*, 2002; Musayev *et al.*, 2003). Two catalytic sites are located at the dimer interface. The first ten and 16 N-terminal amino-acid residues as well as residues 130–175 and 128–175 are missing from monomers *A* and *B*, respectively. The root-mean-square deviation (r.m.s.d.) between the two monomers is 0.40 Å for 131 pairs of C^{α} atoms, with significant differences at the loop and turn regions of residues 45–48, 122–127, 175–179 and 192–200. Fig. 1(*a*) shows a difference Fourier electron-density map (using phases before FMN was added to the model) and Fig. 1(*b*) shows the $2F_{\rm o} - F_{\rm c}$ map of the final model, all calculated around the FMN-binding site.

3.2. Structural comparison

The ePNPOx binary complex with FMN in the tetragonal unit cell is compared with the previously reported ePNPOx binary complex with FMN in a trigonal unit cell (PDB code 1dnl), as well as with the ePNPOx ternary complexes with FMN and PLP in trigonal (PDB code 1g79) and monoclinic (PDB code 1jnw) unit cells. In the trigonal and monoclinic structures, each subunit consists of two domains (domains 1 and 2) that are folded into an eight-stranded β-sheet surrounded by five α-helical structures (Fig. 2*a*). The larger domain 1 is formed by the β-sheets ($\beta1$–$\beta8$) and two of the five α-helices ($\alpha1$ and $\alpha2$). The smaller domain 2 is made up of the three remaining α-helices (helices $\alpha3$, $\alpha4$ and $\alpha5$; residues 122–179). Although the overall topology of the tetragonal structure is identical to the trigonal and the monoclinic structures (Safo *et al.*, 2000), there are some significant differences. In the tetragonal structure, most of the domain 2 residues are disordered and are not included in the structure (Figs. 2*a* and 2*b*). These include residues 130–175 and 128–175 of monomers *A* and *B*, respectively. In addition, the tetragonal structure is missing the first ten and 16 N-terminal residues in monomers *A* and *B*, respectively, while the trigonal structure is missing the first 19

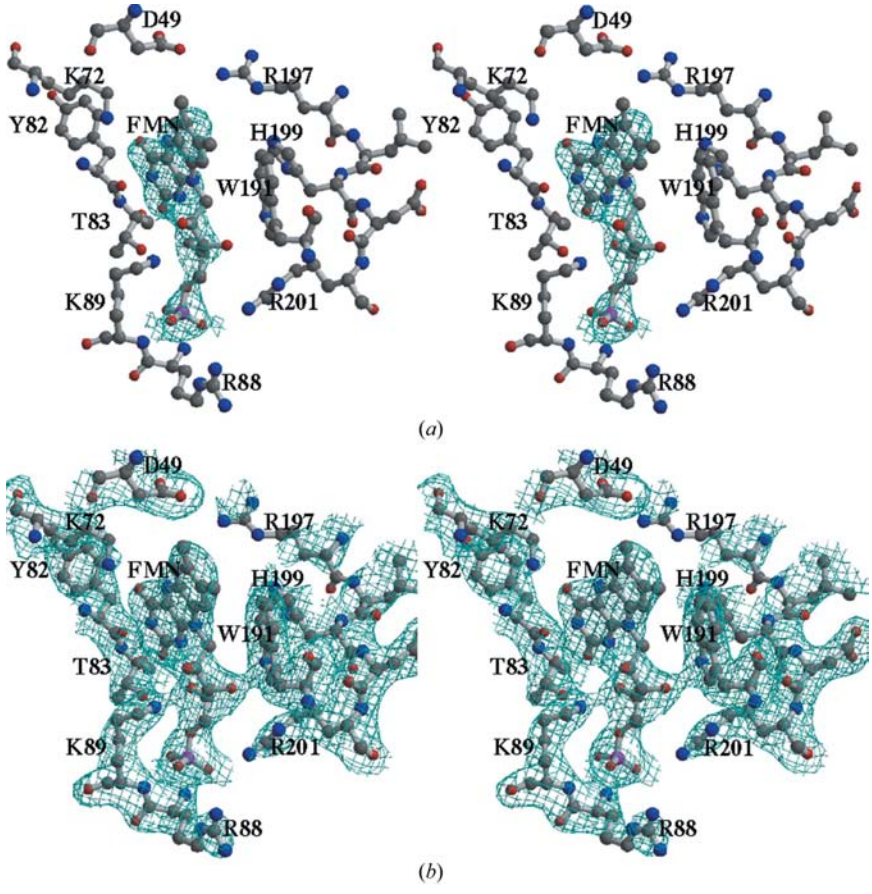

Figure 1
Stereoview of electron-density maps of tightly bound FMN at the active site of ePNPOx in the tetragonal cell. (*a*) $F_{\rm o} - F_{\rm c}$ electron-density map of FMN calculated before FMN was built in the model. (*b*) $2F_{\rm o} - F_{\rm c}$ electron-density map of FMN calculated during the final model refinement. Maps were contoured at 2.5σ and 1.0σ levels, respectively, and superimposed on the final refined model of FMN and selected active-site residues. Residues from monomer *A* include Asp49, Lys72, Tyr82, Thr83, Arg88 and Lys89, while the other residues belong to monomer *B*. Atoms are shown in ball-and-stick representation, with O and N atoms colored red and blue, respectively. The figures were drawn using *BOBSCRIPT* (Esnouf, 1997) and *RASTER3D* (Merritt & Murphy, 1994) and labeled with *SHOWCASE* (Silicon Graphics Inc).

N-terminal residues. In contrast, the monoclinic structure is only missing the first five N-terminal residues (Fig. 2*b*).

The tetragonal dimeric structure superimposes on the trigonal and monoclinic structures with an r.m.s.d. of ∼0.4 Å for 272 pairs of C^{α} atoms using residues 22–45, 49–121, 179–194 and 199–217. If a more stringent criterion for LSQ fitting of 1.0 Å is used, the r.m.s.d. is ∼0.37 Å. The corresponding values between the monoclinic and trigonal structures are 0.20–0.37 Å. The structures are superimposed using the LSQ procedure *LSQKAB* as implemented in the *CCP*4 program suite (Collaborative Computational Project, Number 4, 1994). As shown in Fig. 2(*b*), models from the tetragonal, monoclinic and trigonal crystals fit with minimal deviations, including the FMN. Major differences between the structures occur mainly in turns and loops. The larger values between the tetragonal and the other structures are likely to be a consequence of the low resolution of the tetragonal structure and changes in tertiary structures that result from PLP binding in the trigonal and monoclinic structures, as well as the disorder of domain 2 in the tetragonal structure.

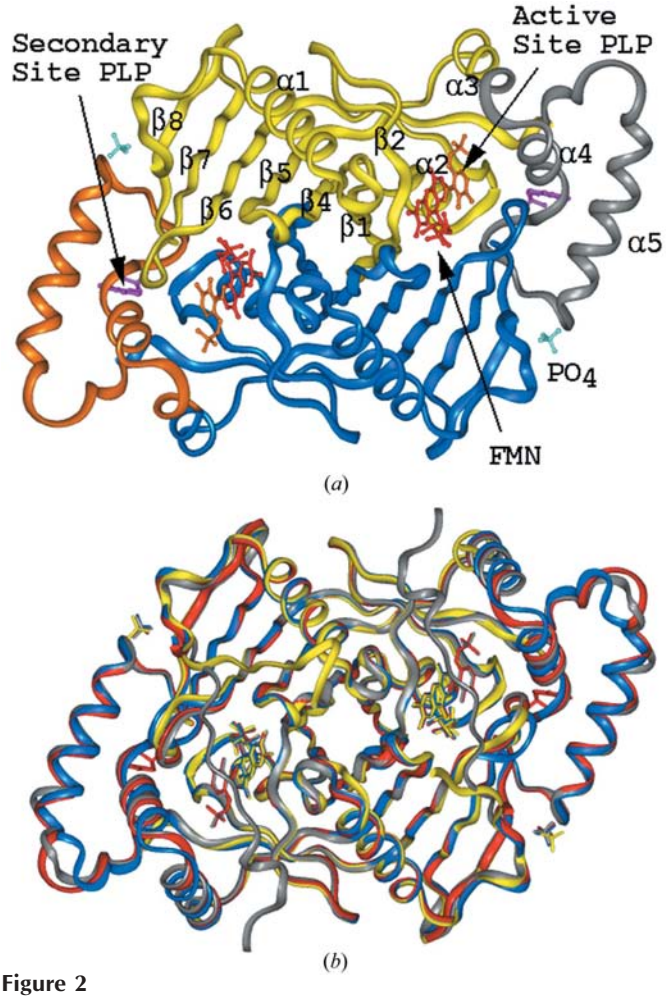

Figure 2
Ribbon diagrams of the dimeric structures of ePNPOx. (*a*) The structure of the ePNPOx ternary complex with FMN and PLP in a trigonal unit cell (PDB code 1g79). Monomer *A* is colored yellow (mostly domain 1) and gray (mostly domain 2) and monomer *B* is colored cyan (mostly domain 1) and orange (mostly domain 2). The FMN (red), PLP (orange and magenta) and phosphate (cyan) molecules are shown as stick models. The secondary structures are labeled for monomer *A*. Note that domain 2 (part of helix α3, helix α4, helix α5 and associated loops; colored gray and orange) is highly disordered and untraceable in the tetragonal structure. (*b*) Least-squares superposition of ePNPOx binary complex with FMN in the tetragonal unit cell (yellow), ePNPOx binary complex with FMN in the trigonal unit cell (cyan; PDB code 1dnl), ePNPOx ternary complex with FMN and PLP in the trigonal unit cell (red; PDB code 1g79) and ePNPOx ternary complex with FMN and PLP in the monoclinic unit cell (gray; PDB code 1jnw). Note that PLP was observed bound at both the active and secondary sites in the trigonal ternary complex. The figures were drawn using *INSIGHT*II (Molecular Simulations Inc.) and labeled with *SHOWCASE*.

3.3. Active site

There are two active sites in the dimeric structure of ePNPOx and each is located at the dimer interface formed by residues from both monomers (Safo *et al.*, 2000, 2001; Salvo *et al.*, 2002; Musayev *et al.*, 2003). The binding of FMN at the active site of the tetragonal structure is identical to those of the monoclinic and trigonal forms (Figs. 2*b* and 3). We have previously discussed the active site in open, partially closed and completely closed conformations when uncomplexed or complexed with PLP (Di Salvo *et al.*, 2002). The PLP is located on the *re* face of N5 of FMN and binds with similar geometry in both the monoclinic and trigonal crystal structures (Figs. 2 and 3). In the trigonal structure without bound PLP, the active site is in an open conformation. Binding of PLP to the trigonal structure causes the C-terminus of helix α3, helix α4, the loop located between these two helices (residues 129–140) and the turn located between the strands β6 and β7 (residues 193–199) to move further toward the active site, resulting in the residues Tyr129, Arg133, Ser137, Arg197 and His199 making interactions with the PLP (Fig. 3*a*). In the monoclinic crystal, although the dispositions of the above active-site residues remain identical and make similar interactions to the bound PLP, the interactions are tighter. Note that these active-site residues are highly conserved among the PNPOx family of enzymes (Safo *et al.*, 2000; Musayev *et al.*, 2003). Interestingly, the N-terminus (residues 14–18) in the monoclinic structure stretches over the mouth of the active site to sequester the bound PLP, with Arg14 and Tyr17 forming hydrogen bonds with PLP (Figs. 2*b* and 3*a*). These interactions have completely closed the active site of the monoclinic structure. In contrast, in the trigonal structure with bound PLP the first residue that could be identified is Gly20 and obviously the bound PLP is only partially sequestered, as described above. There is not a strong conservation of Arg14 and Tyr17 in PNPOx sequences, but other enzymes in the family do show complete conservation of residues that can form hydrogen bonds with the PLP in this extended region of the N-terminus (Safo *et al.*, 2000; Musayev *et al.*, 2003).

Although we could isolate the ternary complex in both trigonal and monoclinic crystal forms, co-crystallization or soaking of the tetragonal crystals with PLP did not result in binding of PLP. The most obvious reason is that most of the residues that help anchor the PLP at the active site, including the domain 2 residues Tyr129, Arg133 and Ser137, are significantly disordered and may not be available to form

interactions with PLP (see below). Also, it is worth mentioning that the trigonal crystal structures that were determined from a crystal either soaked or co-crystallized with PLP show bound PLP at the active site (Safo *et al.*, 2001). In contrast, we only obtained monoclinic crystals when the enzyme is co-crystallized with PLP (Di Salvo *et al.*, 2002). The result suggests that the fold of the N-terminal region over the active site occurs after the PLP binds.

3.4. Putative non-catalytic PLP-binding site and tunnel

In vitro solution studies have shown that PNPOx binds a second molecule of PLP tightly at a putative non-catalytic site on each monomer of the dimer and even though this PLP remains bound during size-exclusion chromatography and purification procedures, it is readily transferred to apo SHMT (Yang & Schirch, 2000; Musayev *et al.*, 2003). It has been pointed out that this non-catalytic site PLP may play a role in channeling a sequestered PLP to vitamin B_6 apoenzymes (Ováldi & Srere, 2000). Interestingly, the trigonal ternary structure shows a second PLP (Safo *et al.*, 2001) bound in a cleft at the protein surface, about 11 Å from the active site, and making interactions with the residues Phe177, Lys159, Lys145, Ser144, Ala141, Gly85, Asn84, Ala29 and Asp26 (Figs. 2 and 3*b*). It is possible this surface-bound PLP may be the non-catalytic PLP observed in solution studies (Yang & Schirch, 2000; Musayev *et al.*, 2003).

All the PNPOx crystal structures show a possible tunnel between the active site and the secondary PLP site, suggesting that PLP formed at the active site may transfer to this putative non-catalytic site without passing though the solvent (Fig. 3*b*). The putative tunnel in the monoclinic and trigonal structures, which is mostly formed by small side-chain residues from domain 2, is however too narrow to allow passage of PLP. Remarkably, the tetragonal structure shows extensive disorder of most of domain 2, resulting in the absence of part of helix α3, helices α4 and α5 and associated loops from the structure (Figs. 2 and 3). Interestingly, domain 2 of the trigonal and monoclinic crystal forms also show flexibility by having high *B* factors compared with the rest of the structure. These observations point to a strong possibility that domain 2 is flexible and can easily rotate to create significant widening of the channel for PLP passage. We have previously proposed, based on the trigonal ternary structure, that domain 2 can rotate to increase the size of the tunnel (Safo *et al.*, 2001). Possible hinge sites by which the domain 2 can rotate are Ser122 and Gly179.

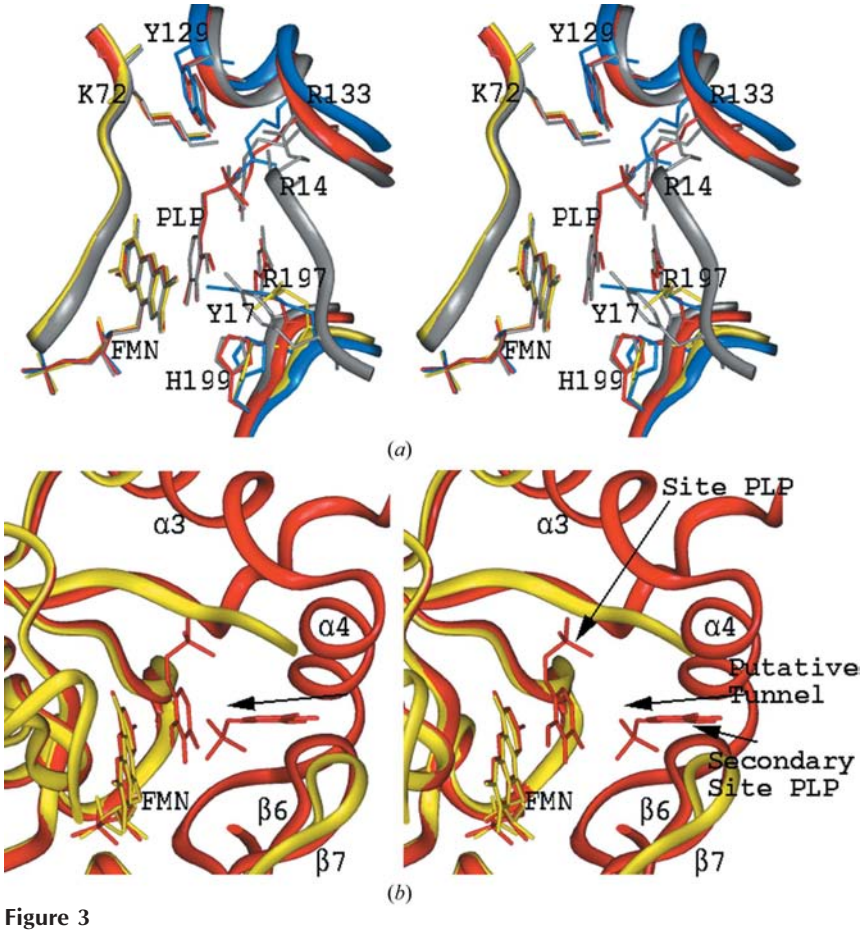

Figure 3
Stereoview of least-squares superposition of the active and putative secondary binding sites of PLP in ePNPOx. (*a*) A close-up view of the active sites of the tetragonal binary complex (yellow), trigonal binary complex (cyan), trigonal ternary complex (red) and monoclinic ternary complex (gray). The protein backbone is shown as ribbons, while the FMN, PLP and active-site residues are shown as stick models. Note the absence of the domain 2 residues Tyr129 and Arg133 in the tetragonal crystal. Also note that the N-terminal residues Arg14 and Tyr17 are present only in the monoclinic crystal. (*b*) A close-up view of the active and secondary PLP-binding sites of the tetragonal binary complex (yellow) and trigonal ternary complex (red), showing the putative tunnel connecting them. Note that disorder of domain 2 in the tetragonal crystal suggest that domain 2 could easily rotate to allow passage of PLP from the active site to the putative non-catalytic secondary PLP site. The figures were generated using *INSIGHT*II and labeled with *SHOWCASE*.

3.5. Mechanistic pathway

Crystallographic as well as biochemical studies of PNPOx with respect to the binary and ternary complexes of the enzyme provide information for the elucidation of the mechanistic activity of the enzyme. The first catalytic step is binding of PNP to the resting binary enzyme, as embodied in the unliganded trigonal crystal form with an open active-site conformation (Fig. 3*a*; structure colored blue). Since we cannot observe the PNP ternary complex because it will react to form the product PLP, our complexes with PLP are inferred to form the same interactions at the active site as PNP. After PNP is bound, the overall PNPOx structure only changes slightly; however, the active-site residues (described above) have moved closer to interact with the substrate as observed in the trigonal ternary complex

(Fig. 3*a*; structure colored red). The active site at this stage could be described as partially but not completely closed and may correspond to the pre-reaction state in which the substrate is positioned correctly. We observed a similar partially closed active-site conformation in the human PNPOx ternary complex, which also crystallized in a trigonal unit cell, but with different space group (Musayev *et al.*, 2003). In a recent study, mutants of the active-site residues (H199A, H199N, D49A, Y17F, R14E and R14M) showed a decrease in affinity, but exhibited considerable catalytic activity, suggesting that these residues are important for binding but play a lesser role in catalysis (Di Salvo *et al.*, 2002). The exception is the active-site residue Arg197, which was found to be important for both binding and catalysis (Di Salvo *et al.*, 2002).

Following the binding of PNP, the N-terminus residues 1–19 that are found to be disordered in the trigonal structure swing over and completely close the active site as observed in the ternary complex of the monoclinic structure (Fig. 3*a*; structure colored gray). In addition, all the active-site residues move even closer and make stronger bonds with the substrate. Significantly, Arg197, which is known to affect catalysis, has become even more ordered and closer to PLP than found in the trigonal ternary structure (Di Salvo *et al.*, 2002). Thus, with the monoclinic structure, we now have the closed form of the enzyme with all active-site residues in contact with the substrate PNP, as well as the exclusion of solvent. Based on these findings, it could be hypothesized that the monoclinic ternary complex represents the reaction or catalytic stage in which PNP is converted to PLP.

In addition to PLP binding (as discussed above), crystal-packing forces in the different crystals are likely to influence the different structural conformations of the flexible regions, including the active site and domain 2 regions. We have previously analyzed packing effects in both the trigonal and monoclinic structures (Di Salvo *et al.*, 2002) and showed that unlike the trigonal structure, the N-terminus of the monoclinic structure is sandwiched between and makes contacts with two crystallographic dimers. Our analysis of the tetragonal structure shows that the N-terminus is largely opened to the solvent. This explains why these residues are only seen in the monoclinic structure. In both the monoclinic and trigonal structures, domain 2, with the exception of a small section of helix α5, is extensively involved in lattice contacts. In contrast, only the N-terminus of helix α3 in the tetragonal structure is involved in any lattice contact, therefore domain 2, which is flexible even in the monoclinic and trigonal structures, cannot pack properly in the tetragonal cell and has thus become disordered in this crystal.

An unanswered question is the location of the tightly bound PLP that can be transferred to apo SHMT. Two possible mechanisms can be postulated. Firstly, PLP could be bound at the non-catalytic site that is removed by 11 Å from the active site after passage through the now enlarged putative tunnel of the tetragonal structure. The active site would be open and the enzyme proceeds with the observed steady-state kinetics when PNP is added as substrate. Secondly, the PLP could be tightly bound at the active site in the closed position after catalysis. In this second mechanism PNP binds at an allosteric site, resulting in a conformational change that results in release of the tightly bound PLP at the active site. This release of PLP permits catalysis to proceed. It may be that the observed non-catalytic PLP or the phosphate-ion-binding site is the allosteric site that binds PNP, which triggers the rotation of domain 2, opening both the tunnel and the active site for release of PLP. We note that the phosphate ion which is located at the same position in all the structures binds in a shallow cleft at the surface of the protein. It is clear from the tetragonal structure that the rotation of domain 2 is important to the release of the tightly bound PLP by either mechanism. What is not clear is the mechanism for the rotation of domain 2 and the location of the tightly bound PLP.

This work was supported by United States Public Health Services Grant DK55648 (to VS).

References

Brünger, A. T. (1992). *Nature (London)*, **355**, 472–475.

Brünger, A. T., Adams, P. D., Clore, G. M., DeLano, W. L., Gros, P., Grosse-Kunstleve, R. W., Jiang, J.-S., Kuszewski, J., Nilges, M., Pannu, N. S., Read, R. J., Rice, L. M., Simonson, T. & Warren, G. L. (1998). *Acta Cryst.* D**54**, 905–921.

Cambillau, C. & Horjales, E. (1987). *J. Mol. Graph.* **5**, 174–177.

Collaborative Computational Project, Number 4 (1994). *Acta Cryst.* D**50**, 760–763.

Di Salvo, M. L., Ko, T.-P., Musayev, J. N., Raboni, S., Schirch, V. & Safo, M. K. (2002). *J. Mol. Biol.* **315**, 385–397.

Di Salvo, M. L., Yang, E., Zhao, G., Winkler, M. E. & Schirch, V. (1998). *Protein Expr. Purif.* **13**, 349–356.

Esnouf, R. M. (1997). *J. Mol. Graph.* **15**, 132–134.

Hill, R. E., Himmeldirk, K., Kennedy, I. A., Pauloski, R. M., Sayer, B. G., Wolf, E. & Spenser, I. D. (1996). *J. Biol. Chem.* **271**, 30426–30435.

John, R. A. (1998*a*). *Comprehensive Biological Catalysis*, edited by M. Sinnott, pp. 84–100. London: Academic Press.

John, R. A. (1998*b*). *Comprehensive Biological Catalysis*, edited by M. Sinnott, pp. 173–200. London: Academic Press.

Merritt, E. A. & Murphy, M. E. P. (1994). *Acta Cryst.* D**50**, 869–873.

Musayev, F. N., Di Salvo, M. L, Ko, T.-P., Schirch, V. & Safo, M. K. (2003). *Protein Sci.* **12**, 1455–1463.

Ováldi, J. & Srere, P. A. (2000). *Int. Rev. Cytol.* **192**, 255–280.

Safo, M. K., Mathews, I. J. N., Musayev, F. N., di Salvo, M. L., Thiel, D. J., Abraham, D. J. & Schirch, V. (2000). *Structure*, **8**, 751–762.

Safo, M. K, Musayev, F. N., Di Salvo, M. L. & Schirch, V. (2001). *J. Mol. Biol.* **310**, 817–826.

Yang, E. S. & Schirch, V. (2000). *Arch. Biochem. Biophys.* **377**, 109–114.

Zhao, G. & Winkler, M. (2000). *J. Bacteriol.* **177**, 883–891.